Available online at www.sciencedirect.com
ScienceDirect
Journal of the European Ceramic Society 30 (2010) 2555–2562
www.elsevier.com/locate/jeurceramsoc

Micro- and macroscopic thermal expansion of stabilized aluminum titanate

Giovanni Bruno [a,*], Alexander Efremov [b], Bryan Wheaton [c], Ivan Bobrikov [d], Valeriy G. Simkin [d], Scott Misture [e]

[a] *Corning SAS, CETC, Avon 77210, France*
[b] *Corning OOO, CSC, St. Petersburg 194021, Russia*
[c] *Corning Inc., CS&S, Corning, NY 14831, USA*
[d] *JINR, FLNP, Dubna 141980, Russia*
[e] *Alfred University, NY 14802, USA*

Received 9 December 2009; received in revised form 21 April 2010; accepted 26 April 2010
Available online 1 June 2010

Abstract

The lattice expansion of aluminum titanate (AT) obtained by firing a mixture of alumina, rutile, strontium and calcium carbonate and silica was measured using neutron and laboratory X-ray diffraction. The microscopic data are compared with macroscopic measurement completed by dilatometry.

A powder and a compact rod sample were compared to assess the influence of micro residual stresses locked into the solid structure at grain level, which could possibly be relieved upon grinding.

Results show good correlation between neutron and X-ray diffraction techniques. They also show that a compact material behaves differently than a powder, contrary to what happens for other porous ceramics such as cordierite. The integrity factor model was used to rationalize the results and predict grain level stresses in all crystal directions and all phases (AT, Strontium aluminum silicate, alumina and residual glass). Calculation show that the AT *c*-axis is always under compression while all other crystal directions and phases are under tension. Those micro-stresses do not undermine the macroscopic mechanical properties of the material and confer to it its interesting properties like low thermal expansion and enhanced strain tolerance.

Keywords: Thermal expansion; Aluminium titanate; Neutron diffraction; X-ray diffraction; Integrity factor; Strain conversion factor; Micro-stresses

1. Introduction

Aluminum titanate (AT) is a material of great interest for diesel particulate filter and many other environmental applications.[1] As the most thermal shock resistant ceramic known, AT is relevant for industrial applications in the form of highly porous and microcracked monolithic bodies.[2] Recent compositions and heat treatments have allowed obtaining stable compounds with high mechanical strength In fact, in order to stabilize the microstructure with respect to thermal cycles, mullite and other additives are often used.[3] A typical X-ray diffraction pattern with the corresponding peak indexing is shown in Fig. 1. The glass content is larger than for instance in cordierite-based porous ceramics (also widely used for environmental applications) and is estimated to be around 4%.

It has also been well established that extruded AT exhibits a unique structure along the extrusion axis.[4] However, while the macroscopic CTE (as measured by dilatometry) has been characterized extensively,[5,7] very little is known on the lattice CTE components.[8] This is particularly true for industrially relevant materials, which are particularly interesting for their superior mechanical, thermal and stability properties, as opposed to model aluminum titanate.[7,9] The anisotropy of the lattice CTE is believed to be the source of internal micro-stress and microcracking at the grain level,[5,10] which confer to AT its attractive thermal shock resistance properties. In order to understand the behaviour at microstructural level, we have undertaken an extensive study of the microscopic expansion of AT using laboratory X-rays and neutron diffraction techniques. Neutron diffraction

* Corresponding author at: Corning Inc., CS&S, SP FR06, 14831 Corning, NY, USA. Tel.: +1 607 9741421; fax: +1 607 9742383.
E-mail address: brunog@corning.com (G. Bruno).

0955-2219/$ – see front matter © 2010 Elsevier Ltd. All rights reserved.
doi:10.1016/j.jeurceramsoc.2010.04.038

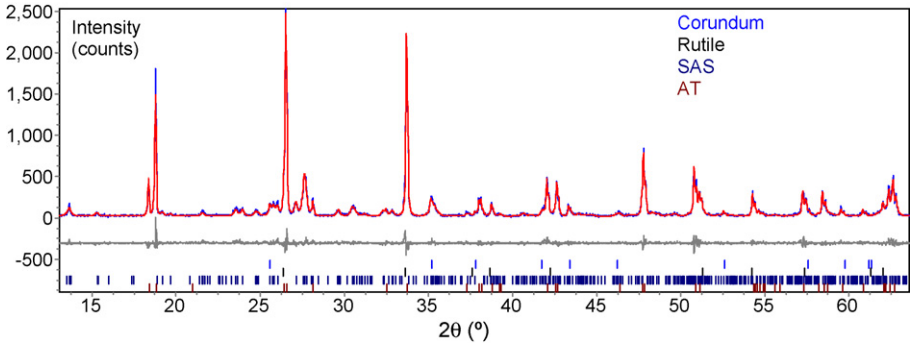

Fig. 1. X-ray diffraction pattern of aluminium titanate with Rietveld refinement. The residual is shown below the diffraction pattern and the Al_2O_3, TiO_2, SAS and AT phases are indicated by the tick marks (the legend and the ticks are in the same order).

offers the advantage of large penetration depths and the ability of accurately measuring bulk specimens without unwanted surface effects.

The specific U-shape of macroscopic dilation vs. temperature curve observed in low CTE ceramics (e.g. cordierite, AT, β-eucryptite)[6,8,11] gives a very clear indication of the temperature at which thermal microcracks can be considered healed and the material expands like a compact body.[6,8] This effect in AT is much clearer than in other materials. Of key importance in modelling the thermo-mechanical behaviour is the knowledge of the crystal lattice properties *vs*. bulk properties.[11,12]

In this paper we will show how the global macroscopic and the phase-specific lattice (microscopic) expansions combine with our simulation work to yield the lattice micro-stresses, which in turn possibly influence the mechanical and physical properties at room and high temperature.

2. Experimental

Samples were prepared by extruding a batch mixture of titania, alumina, silica, strontium and calcium carbonates and binder.[13] The composition was dried and then fired at temperatures exceeding 1450 °C, with both heating and cooling done in ambient atmosphere with rates not exceeding 5 °C/min. The specimens had the form of a rod with about 1 m length and 10 mm diameter. Powders were extracted from pieces of the same rod by (alumina) ball milling.

The microstructure of this material is well known from microscopy work.[3,4] An X-ray diffraction pattern of the compound obtained is shown in Fig. 1. Extracted from Rietveld refinement, it contains the phases reported in Table 1 with their approximate abundance in weight percent: Aluminum Titanate (73), SAS (22), Corundum (5) and Rutile (<0.5). From microscopy work (see[13]) the AT grain size diameter ranged from 3 to 10 μm. The crystallographic database files used for the refinement are also reported in Table 1.

Table 1
Phase composition of the AT compound used in this work.

Phase	%wt	ICSD File
AT	71	2759
Al_2O_3	5	60419
SAS	22	97264
TiO_2 (rutile)	<0.5	34372
Glass	<2	–

AT: aluminum titanate; SAS: strontium aluminum silicate.

The macroscopic dilation of the material has been measured at Corning's research laboratories in Painted Post, NY using conventional dilatometry on a Netzsch DL402 single pushrod dilatometer. This is equipped with silica sample holder and pushrod, allowing easy calibration up to 1000 °C. A small rod with 50 mm length was used for macroscopic dilation measurements. The macroscopic dilation of the rod is given in Fig. 2 (it is very similar to the curves shown in[14]). It was calculated using the formula

$$\varepsilon = \frac{\Delta L}{L_0} \tag{1}$$

where $L = L(T)$ length at temperature T and L_0 = initial length at room temperature.

The porosity of the sample was measured by mercury intrusion, using an Autopore 9520 from Micromeritics. The global porosity was 50% and the mean pore size about 20 μm.

High-temperature diffraction experiments have been carried out at: (1) the Frank Laboratory for Neutron Physics, FLNP, Dubna, Russia, on the beamline HRFD and (2) the X-ray diffraction laboratory at Alfred University, NY, USA.

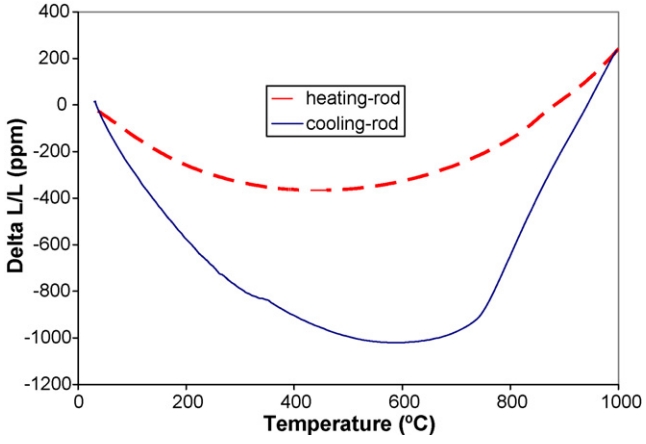

Fig. 2. The macroscopic dilation of a compact rod of AT (see also[13]). The heating and cooling branches are indicated.

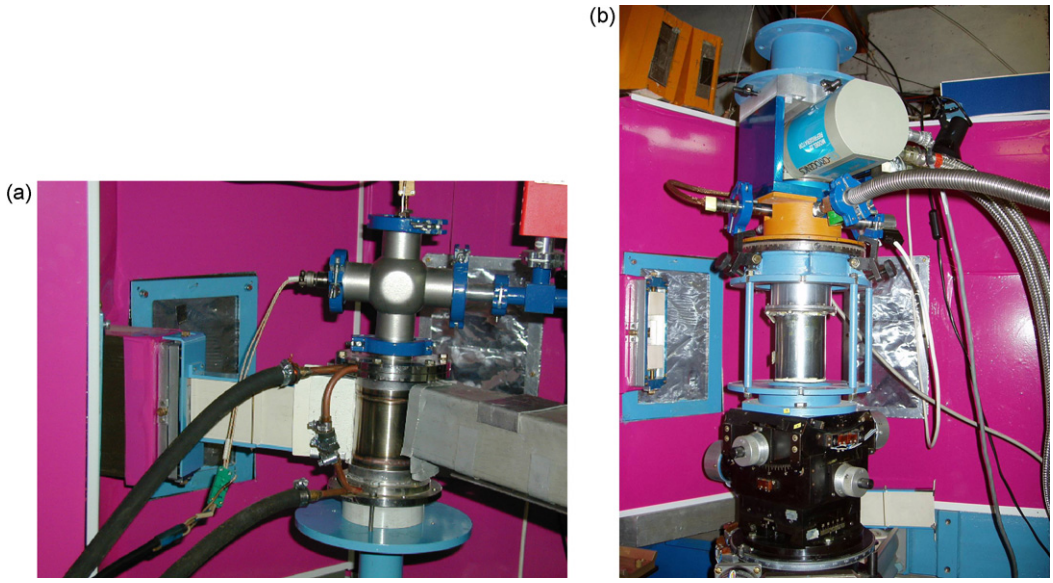

Fig. 3. The furnace (a) and the closed cycle refrigerator (b) used on HRFD. The different detector banks are also visible (covered by aluminium foils).

Neutron experiments employed the reverse time-of-flight (RTOF) technique[15] to obtain very good *d*-spacing resolution. This consists of subtracting two out-of phase medium resolution spectra to obtain a smaller peak width ω thereby improving the peak figure of merit f[16]

$$f = \frac{I}{\omega^2} \tag{2}$$

where I is the peak intensity. On HRFD, a furnace capable of 800 °C and a closed cycle refrigerator capable of liquid helium temperatures (~10 K) have been used in two separate sets of measurements. They are depicted in Fig. 3.

Neutron diffraction data were collected on two samples (powder and solid rod, in the form of a small piece with ~20 mm length) at fixed angles on several detector banks. For ToF diffractometers, the time of flight (t) spectra are converted into *d*-spacing by[17]

$$2d \cdot \sin\,\theta = \frac{h \cdot t}{m \cdot L} \tag{3}$$

where h is the Planck's constant, m the neutron mass and L is the path length. The counting time per point was around 2 h, providing data of sufficient accuracy to determine the lattice expansion for aluminium titanate and the minor phase alumina. The SAS phase was inserted in the Rietveld fit but, due to the large background typical of Reverse ToF spectra, no reliable result was obtained. In the following, only the AT lattice expansion will be discussed. Indeed it is the most relevant for our discussion and conclusions.

High-temperature X-ray powder diffraction (HTXRD) was carried out using a Siemens θ–θ D500 diffractometer equipped with a Braun position sensitive detector and custom high-temperature furnace,[18] using Co Kα radiation with an iron filter. The X-ray diffractometer is shown in Fig. 4. The HTXRD temperature accuracy was calibrated using NIST-ICTA differential thermal analysis standards including KNO_3, $KClO_4$, Ag_2SO_4, K_2SO_4, K_2CrO_4, and $BaCO_3$ that allow calibration up to approximately 800 °C. Higher temperature calibrations were made using the melting points of high-purity Ag, Au, and Ni metals, as well as the phase transitions of $BaSO_4$ and $Ca_3(PO_4)_2$ which show solid-state transitions at 1168 and 1475 °C, respectively. The high-temperature experiments were carried out using a heating rate of 30 °C/min, with measurements made isothermally on reaching each setpoint temperature. The PSD has a resolution of about 0.02° in 2θ (typical for laboratory XRD equipments). It was scanned along 2θ using a scan rate of 5° 2θ/min. In this way, XRD patterns were collected over the 2θ range 5–90°. Each complete XRD pattern collection time was ~17 min. AT, SAS and residual alumina were easily modelled using Rietveld analysis, while the Rutile phase was barely visible.

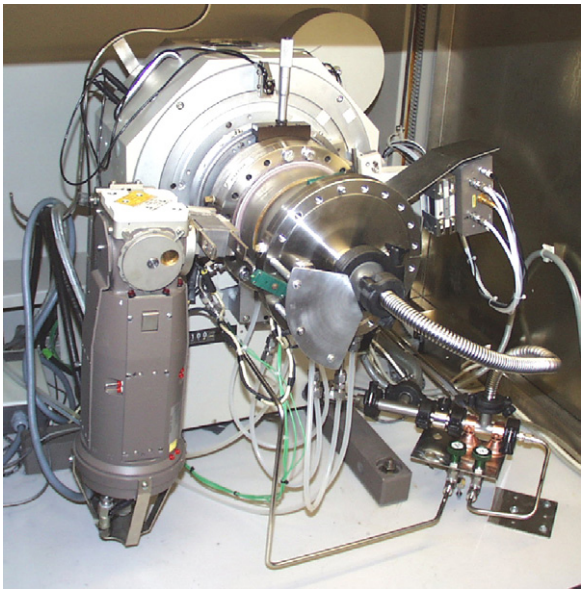

Fig. 4. The high-temperature X-ray diffraction system at Alfred University, Alfred, NY, USA.

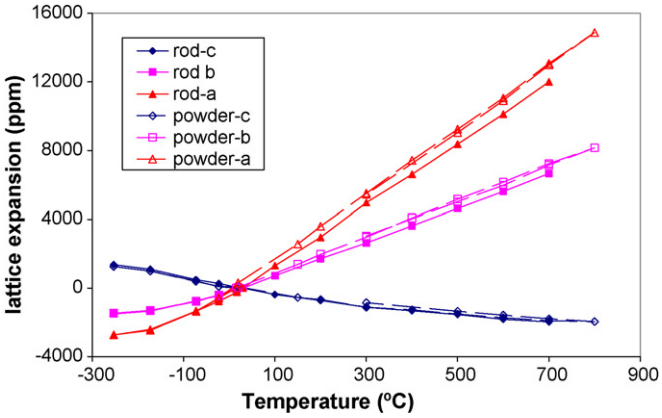

Fig. 5. The expansion of aluminum titanate as a function of temperature for the solid rod and powder samples as measured by neutron diffraction (Dubna, Russia); both heating and cooling ramps are shown.

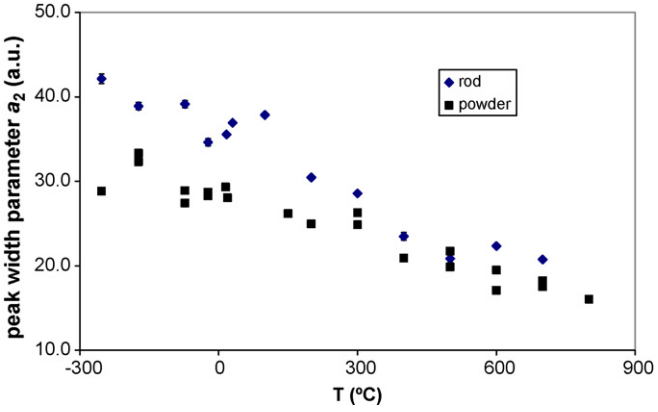

Fig. 6. The (relative) peak width parameter a_2 of aluminum titanate as a function of temperature for the compact rod and the powder samples as measured by neutron diffraction; error bars are included in the symbols.

The ICSD files[19] indicated in Table 1 were used for phase analysis. In particular, the convention used by Morosin and Lynch[20] has been adopted, where the *c*-axis has negative expansion and the *b*-axis has the maximum positive expansion.

We will see that in the modelling section the SAS lattice expansion will be properly used.

3. Results

3.1. Neutron diffraction

The dilations of the three AT crystal axes are shown in Fig. 5. They are calculated similarly to Eq. (1) as:

$$\varepsilon_i = \frac{\Delta d_i}{d_i} \quad i = a, b, c \tag{4}$$

where d_i are the lattice parameters a, b, c and the suffix 0 stands for the room temperature value. Even if a small shift can be noticed for the powder lattice parameters, when comparing the furnace and cryostat data, the dilation data collected during different runs look very consistent. No or very little hysteresis can be detected in any of the three crystal directions. It must be noted that the *c*-axis contraction is much smaller than the *a*- and *b*-axis expansions.

It can be seen that the thermal expansion in the furnace experiment is always slightly larger for the powder than for the rod, while at sub-ambient temperatures the two samples have very similar dilations. This indicates that microcracking is complete and the rod expands like a loose powder (see also[21]).

Interestingly enough, the *a* and *b* dilations look linear in the high-temperature regions while they deviate from linearity at low temperatures.

The fitting program MRIAWIN[22] used at Dubna defines the functional dependence of the integral peak width ω on the d-spacing d in the form of

$$\omega = (a_1 + a_2^2 \cdot d^2)^{1/2} \tag{5}$$

The parameter a_1 is a diffractometer constant, so the most important parameter for our purposes is the term a_2, the integral peak width. Fig. 6 shows the variation of the integral peak width parameter a_2 as a function of temperature for both powder and solid samples. We notice that the rod always has a larger integral width parameter and the difference between the two samples increases at low temperatures. Moreover, the integral width parameter increases with decreasing temperature.

3.2. X-ray diffraction

Fig. 7 displays the lattice expansion data for aluminum titanate determined by X-ray diffraction. It can be seen that all expansions follow more or less a parabolic law, with a very weak quadratic dependence. The large discrepancy with the findings of Fig. 5 is due to the different temperature range used in the two experiments.

For the X-ray data, the AT and alumina were detected and fitted by means of the commercial Rietveld fit program Topas.[23] Fig. 8 shows the lattice dilation as a function of temperature for the alumina.

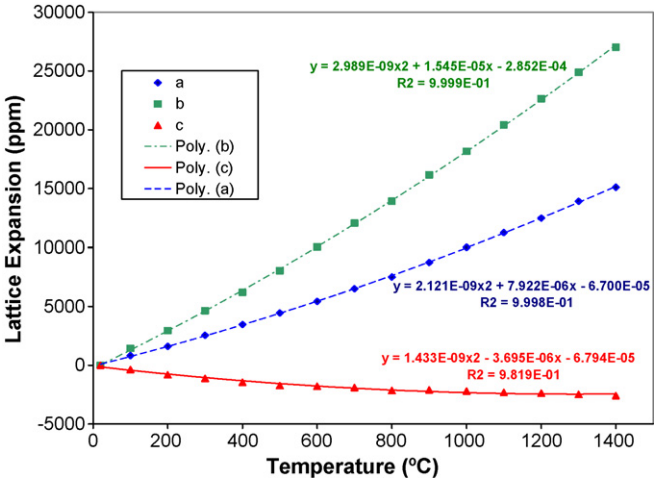

Fig. 7. The expansion of aluminium titanate as a function of temperature for the powder sample, as measured by X-rays; the fit lines (parabolae) and the fit parameters are shown.

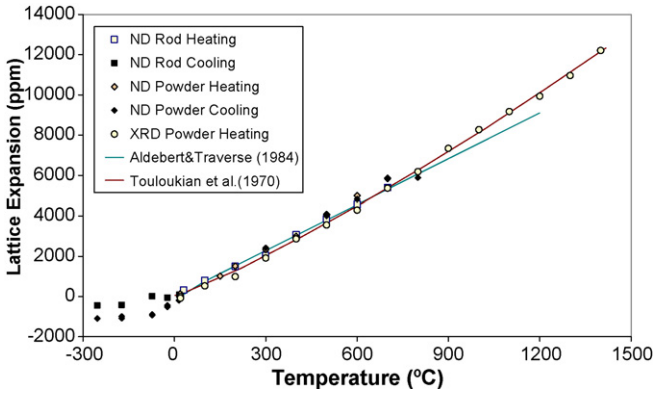

Fig. 8. The *a*-axis expansion of the alumina phase as a function of temperature for the powder sample. All available data are compared with literature.

Indeed, the Al_2O_3 phase was used as a calibration material to monitor for possible sample or beam movements. The agreement between literature values,[24,25] neutron and X-ray diffraction data is very good, as shown in Fig. 8. We can therefore state that no significant sample displacement occurred during the measurements that was not accounted for in the Rietveld refinement.

The full width at half maximum (FWHM) of the XRD peaks were modelled with Topas using a Pearson VII function resulting in a smoothly varying function with 2-θ described by

$$\text{FWHM} = c_1 + \frac{c_2}{\cos\theta} + c_3 \tan\theta \tag{6}$$

Fig. 9 displays the peak width parameter c_1, as a function of temperature for the powder sample as measured by XRD, showing a similar trend to the neutron data displayed in Fig. 7, possibly including levelling off below ~300 °C.

4. Modeling and Discussion

The macroscopic dilation curve of AT of the rod (Fig. 2) can be quantitatively reproduced and rationalized by introducing the integrity factor model,[11,12] see Fig. 10. This model is a generalization of Turner's model for the average CTE of multiphase isotropic materials[26] to orthotropic polycrystalline materials with texture, connected pores and thermal microcracking.

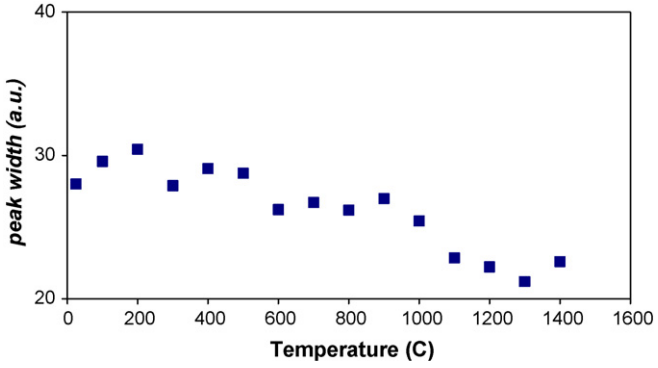

Fig. 9. The peak width parameter c_1 of aluminium titanate as a function of temperature for the powder sample, as measured by XRD; the error is contained in the symbol.

The integrity factor model defines the bulk thermal expansion ε as a function of lattice stress-free thermal expansion (ε_i), elastic properties (E_i), and weighted contribution (V_i), of the various AT crystal directions ($i = a,b,c$) and phases present in the material ($i = (a, c)_{Al_2O_3}$, glass, $(a,b,c)_{SAS}$):

$$\varepsilon = \frac{\sum \varepsilon_i V_i E_i w_i}{\sum V_i E_i w_i} \tag{7}$$

The sum in Eq. (7) can be carried over all crystal directions and possible (an)isotropic phases. As mentioned before, V_i is a weight fraction that takes into account the crystallographic texture and the volume fraction of the grains oriented in the principal crystal directions, w_i is the quoted integrity factor. The latter describes the variation of the lattice contribution to bulk properties due to thermal microcracking.

By definition, the conditions $\Sigma V_i = 1$ and $0 \le w_i \le 1$ hold. Let us note in Eq. (7) that the open porosity does not influence thermal expansion because $E_{void} = 0$.

By means of Eq. (7) we can, for instance, calculate the contribution of the three crystallographic axes to the bulk CTE of AT, assuming that $w_i = 1$ holds at very high temperatures (in our case 1000 °C). If we average the neutron diffraction *a*,*b*,*c* lattice expansions shown in Fig. 5, the calculated behavior of non-microcracked AT upon cooling looks like the dashed line in Fig. 10. Here we used molecular dynamics calculations of lattice constants, experimental evidence of the structural isotropy (image analysis, not shown), and experimental data for phase composition. The agreement between calculations and the experimental macroscopic dilation (dotted curve) at high temperature can be improved by introducing the further assumption that the AT *b*-axis is disconnected at high temperatures.

At this point we can estimate the AT lattice ($i = a,b,c$) and the minority phase average micro-stress ($i = Al_2O_3$, glass, SAS). By multiplying Eq. (7) by the right-hand side denominator and by using phase average stress balance $\sum V_i \cdot w_i \cdot \sigma_i = 0$,[11] the phase average stress is given by

$$\sigma_i = A \cdot w_i \cdot (\varepsilon - \varepsilon_i) \cdot E_i \tag{8}$$

The phase average micro-stress is due to the expansion mismatch between each individual phase and the bulk solid. The factor *A* has to be inserted for the sake of mathematical rigor, since Eq. (7) and the stress balance condition hold if we multiply them by an arbitrary factor. Therefore, *A* is common to all phases and can be interpreted as a macroscopic material structural parameter that quantifies the influence of the mismatch between the phase and the bulk strains on the average phase micro-stress. We will refer to *A* as the *strain conversion factor*, since in this way:

(i) It will indeed be a global parameter
(ii) It will distinguish itself from the integrity factor, which is phase-specific and solely related to the connectivity of each phase to the rest of the body (microcracking).

On cooling from the stress-free reference temperature T_r (1000 °C in our case) the AT *c*-axis, which has negative CTE,

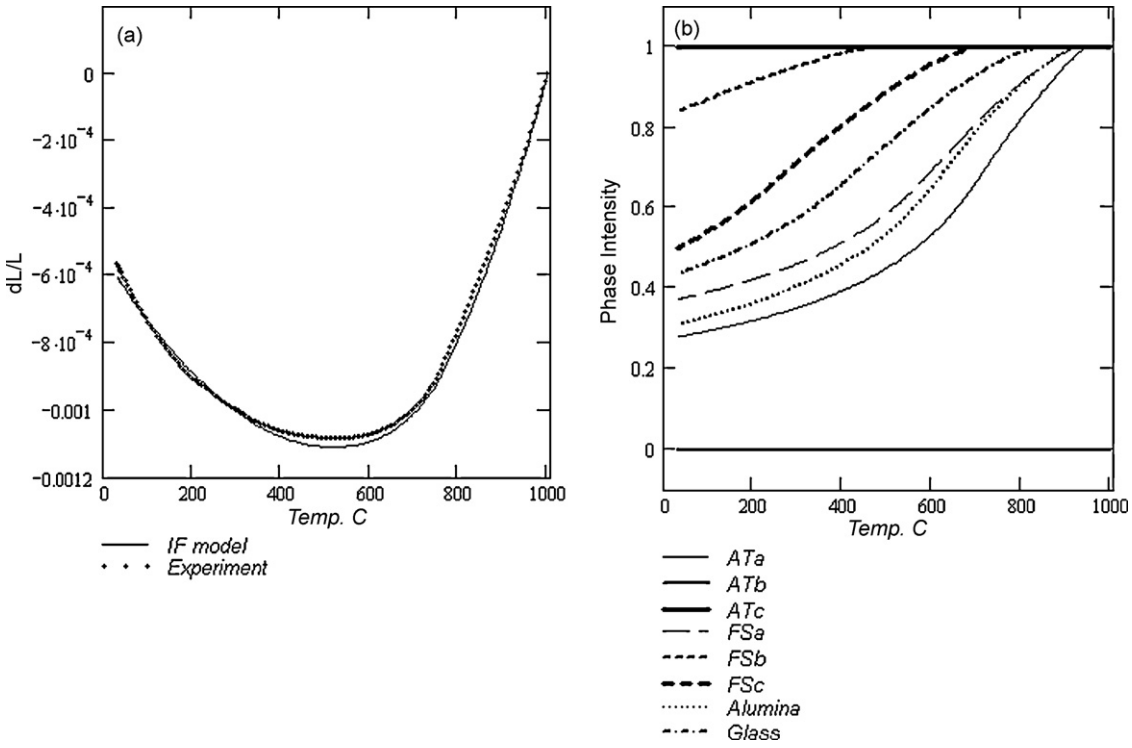

Fig. 10. The simulation of the macroscopic dilation of aluminum titanate (a), and the calculation of the integrity factors with $(\sigma_c)/E_d = 0.15\%$ (b).

expands ($\varepsilon_c > 0$) while the sample contracts as a whole ($\varepsilon < 0$). We can then deduce from Eq. (8) that the *c*-axis is always under compression. From the stress balance equation we conclude that the phases and crystal lattices with positive thermal expansions must be under tension on a microscopic level.

We can suppose that microcracking occurs when the lattice tension exceeds some microscopic threshold value σ_c. Since the compression strength is much higher than the tensile strength (also at macroscopic level) we can safely assume that the *c*-axis disconnection does not occur as a function of temperature and therefore $w_c = 1$, at all temperatures.

In this case, the integrity factor decreases according to the power law

$$w_i = \begin{cases} 1 & \sigma_i < \sigma_c \\ \left(\dfrac{\sigma_c}{\sigma_i}\right)^{2/3} & \sigma_i > \sigma_c \end{cases} \quad (9)$$

This model was found empirically for a single phase material like cordierite, where the temperature dependence of the integrity factor could be extracted directly from the micro- and macroscopic CTE curve. Generally, the exponent value would depend on the grain size and shape distribution whereas the modulus of rupture would depend on the nature of the intergranular medium; however, such an analysis goes far beyond the scope of this paper. Here we simply adopt the empirical power model assuming that σ_{crack} is an adjustable parameter to fit to the bulk thermal expansion of AT and that it is a microscopic parameter common to all phases, for simplicity.

The calculation of the integrity factor for all phases and all crystal directions is shown in Fig. 10b. This shows that for the AT phase $w_b = 0$ and $w_c = 1$ at any temperature, whereas the *a*-axis for AT, the alumina and the glass, all have a different contribution to microcracking (in decreasing order respectively: AT-*a*, alumina, glass).

Similarly, according to Fig. 10a, the integrity factor model yields excellent agreement between simulations and experimental data. The model parameters $(\sigma_c)/E_i = 0.15\%$ and stress-free temperature $T_r = 1004\,^{\circ}C$ have been used in the fitting procedure. These values can be considered, respectively, as estimates of the microscopic strain tolerance and the temperature for grain sliding to freeze. This grain sliding phenomenon can be considered responsible for the release of anisotropic grain stresses at high temperature.

Both grain and pore structure would influence the conversion of thermal strain mismatch into local micro-stress. For example, in a laminated (non-porous) structure *A* equals 0 in the direction perpendicular to the layer planes. In this direction the expansion of each layer does not constrain the expansions of the others. On the contrary, the A parameter equals 1 in the parallel direction where the expansions are fully constrained. With this interpretation, we can assume that the parameter *A* varies in the range $0 < A < 1$ and depends on the orientation when the grain structure is anisotropic. The closer *A* is to 1, the higher the necessity of transforming strains into stresses. For a random crystal orientation one would expect $A = 1/3$. To check this statement, the average stresses in a matrix of axisymmetric polycrystals (e.g. hexagonal crystals) were simulated by FEM. Each crystal was modeled as a cubic element oriented evenly along the *XYZ* directions, as suggested in Ref. [11]. By letting the elastic constants of the grains vary in a wide interval, the calculated *A* values fell near 1/3, in more than 90% of the cases. This confirmed therefore the

reasonable assumption of $A = 1/3$ and that the force (and stress) balance condition holds. Moreover, it implies that the dependence of the stress values on the elastic constants is low, which justifies the use of molecular modeling calculations. It is well known that the single crystal elastic constants of AT are thus far not available.[27]

It is also expected that porosity and microcracking would decrease A, i.e. they would allow deformation and avoid the formation of intergranular stresses. Moreover, the Young's modulus in a porous body is smaller than any of its crystallographic axes, i.e. $E_P < E_i$. An effective Young's modulus must be inserted in Eq. (8). This creates a beneficial effect on the internal microstresses: assuming that the thermal strain mismatch of Eq. (8) is shared between rigid dense grains and the soft porous medium proportionally to their compliances, we can estimate a smaller stress value in a porous material, given by

$$\sigma_i = A \cdot w_i \cdot (\varepsilon - \varepsilon_i) \cdot \frac{2E_i E_P}{E_i + E_P} \tag{10}$$

The elastic properties of a porous structure (the porosity P and the pore morphology m), can be related to those of the dense material (E_d), for example by power law[28]

$$E_P = E_d \cdot (1 - P)^m \tag{11}$$

Hence E_P would change as soon as the pore structure changes e.g. due to microcracks.

Fig. 11 presents the average micro-stresses as a function of temperature, calculated by Eq. (10). It clearly shows the huge difference of stress development in the different phases on cooling,

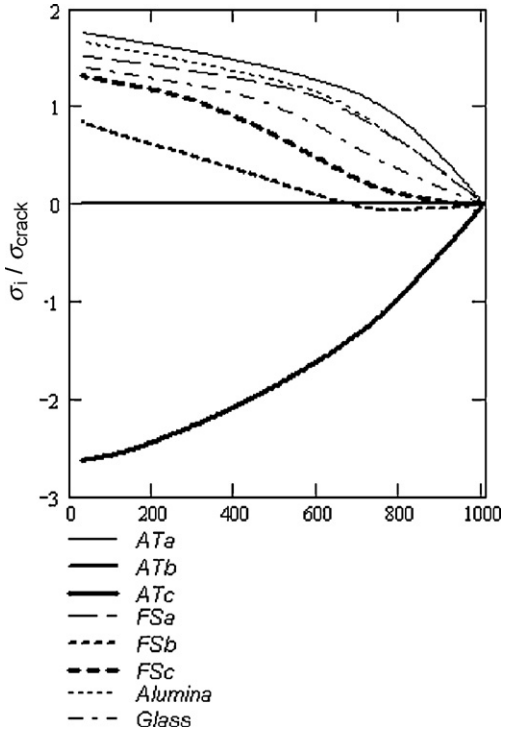

Fig. 11. Application of Eq. (10) for estimating the micro-stress during cooling of AT, SAS Feldspar, Al_2O_3 and glass as a function of temperature. This includes the effect of gradual microcracking. For simplicity E_d and E_i are assumed equal; other structural parameters assumed are: $P = 0.50$, $m = 2.4$.

most probably due to microcracking: Besides the AT a-axis, the alumina, SAS feldspar and the glass are subjected to significant microcracking, due to the presence of micro-stresses.

Such a variation in micro-stresses can be detected by comparing the AT dilations in rod and powder samples (see Fig. 5) and their peak width (Fig. 6). The dilation of the rod is more constrained and therefore the strain difference to the powder is negative. Indeed, calculations (see Fig. 11) show that the rod, the a and b axes experience higher tension and the c-axis higher compression than those in the powder, implying $A_{rod} > A_{powder}$. Therefore, a possible way to investigate experimentally the dependence of A on T would be to prepare different particle size powders and different porosity rods and to evaluate a stress-free sample to compare with all others. This is certainly a subject for further research.

Moreover, we notice that large micro-stresses build up upon cooling until microcracking occurs. At this point (say 800–750 °C) micro-stresses start to be relieved and may end up lower at RT than at 800 °C.

Finally, we notice that the increasing importance of microstress and microcracking during cooling is reflected in the behavior of the integral peak width (Fig. 6). In spite of the fact that the instrumental contribution is difficult to deconvolute from that of the sample, the (total) peak width shows that lattice and/or orientation mismatch increases on cooling. While more and more grains disconnect and therefore release their stress, the diffraction peaks become wider. We could expect that eventually a combination of stressed ($w_i = 1$) and stress-free ($w_i = 0$) crystallites produces a bimodal distribution of lattice parameter, where the diffraction peak separation increases on cooling due to micro-stress (Fig. 11).

5. Conclusions

In this paper the lattice expansion of industrially relevant AT containing residual glass, feldspar and alumina has been investigated by neutron and laboratory X-ray diffraction. A solid rod and loose powder were chosen. The neutron and X-ray results are in excellent agreement, and tracking both peak widths and dilation differences between the two samples suggested that more strain mismatch between grains is present in the solids than in the powders. This mismatch increases with decreasing temperature. This implies that the rod is less 'stress-free' than the powder, in spite of porosity and microcracking. However, upon going to sub-zero temperatures, the strain difference seems to vanish, and microcracking becomes predominant in relaxing internal stresses in the rod.

The use of the integrity factor model has allowed the calculation of the contribution of microcracking to the macroscopic dilation of AT. On the basis of lattice data, the dilation of the equivalent ideal non-microcracked material could be simulated. By subtracting this ideal behavior from the macroscopic dilation curve, the effect of thermal microcracking (as a function of temperature) on the total dilation could be assessed. Although based on the assumptions that the AT c-axis is always connected and the b-axis is always disconnected from the rest of the body (i.e. $w_c = 1$ and $w_b = 0$ at any temperature), the present results

are self consistent. Moreover cross-check done in parallel work has shown that these two hypotheses are well corroborated by experimental data.

The model has also allowed calculating micro-stresses in all phases. While this grain stress strongly depends on the reference stress-free temperature T_r, its development as a function of temperature for a particular case of $T_r = 1000\,^{\circ}C$ indicates that the AT *c*-axis undergoes strong compression while the AT *a*-axis is in tension, similar to the feldspar, residual alumina and glass. These levels of compression and tension are mitigated by microcracking, and the room temperature residual stress is lower than that of a solid body. This demonstrates a further advantage of a microcracked material, in addition to its attractive thermal expansion properties and thermal shock resistance.

Acknowledgements

Suresh Gulati (Corning Inc, NY, USA) and Anatoly Balagurov (FNLP Dubna, Russia) carefully read the manuscript and provided very precious suggestions; Jim Webb, Michele Fredholm, Jim Dickinson, Adama Tandia, Daniela Lavric, Andrey Levandovskyi and Patrick Tepesch (all Corning Inc.) provided data and very useful discussion.

Beamtime at IBR-2 reactor at JINR in Dubna, Russia is kindly acknowledged.

References

1. Thomas HAJ, Stevens R. Aluminium titanate—a literature review, part 2—engineering properties and thermal stability. *Br Ceram Trans J* 1989;**88**:184–90.
2. Lu TJ, Fleck NA. The thermal shock resistance of solids. *Acta Mater* 1998;**46**:4755–68.
3. Korim T, Kotsis I. Effects of additives in the properties of Al_2TiO_5 ceramics. *Meter Sci Forum* 2003;**414–415**:117–20.
4. Qian DF, Ohya Y, Nakagawa Z, Hamano K. Orientation of grains in aluminum titanate ceramics prepared from the agglomerates of alumina and titania. *J Ceram Soc Jpn* 1995;**103**:1022–6.
5. Thomas HAJ, Stevens R. Aluminium titanate—a literature review. Part 1. Microcracking phenomena. *Br Ceram Trans J* 1989;**88**:144–51.
6. Turner SR, Taylor R. Thermophysical properties of aluminium titanate. *High Temp High Press* 1991;**23**:445–53.
7. Skala RD, Li D, Low IM. Diffraction, structure and phase stability studies on aluminium titanate. *J Eur Ceram Soc* 2009;**29**:67–75.
8. Buessem WR, Thielke NR, Sarakauskas RV. Thermal expansion hysteresis of aluminum titanate. *Ceramic Age* 1952;**60**:38–40.
9. Bayer G. Thermal expansion characteristics and stability of pseudobrookite-type compounds, Me_3O_5. *J Less Common Metals* 1971;**24**:129–38.
10. Cleveland IJ, Bradt RC. Grain size/microcracking relations for pseudobrookite oxides. *J Am Ceram Soc* 1978;**61**:478–81.
11. Efremov AM. Impact of domain anisotropy on CTE of isotropic microcrystalline material. *Phil Mag* 2006;**86**:5431–40.
12. Bruno G, Efremov AM, Clausen B, Balagurov AM, Simkin V, Wheaton BR, Webb JE, Brown DW. On the stress free lattice expansion of cordierite. *Acta Mater* 2010;**58**:1994–2003.
13. Ogunwumi SB, Tepesch PD, Chapman T, Warren CW, Melscoet-Chauvel I, Tennent DL. Aluminum titanate composition for diesel particulate filters. Proceedings SAE world congress 2005, SAE 2005-01-0583.
14. Backhaus-Ricoult M, Glose C, Tepesch P, Wheaton BR, Zimmermann J. ICCAC Conference Proceedings (2010), ACERS - in publication.
15. Aksenov VL, Balagurov AM, Simkin VG, Bulkin AP, Kudrjashev VA, Trounov VA, Antson O, Hiismaki P, Tiitta A. Performance of the high resolution Fourier diffractometer at the IBR-2 pulsed reactor. *J Neutron Res* 1997;**5**:181–200.
16. Johnson MW, Daymond MR. An optimum design for a time-of-flight neutron diffractometer for measuring engineering stresses. *J Appl Cryst* 2002;**35**:49–57.
17. Copley JRD, Udovic TR. Neutron time-of-flight spectroscopy. *J Res Nat Bureau of Standards* 1993;**98**:71–87.
18. Misture ST. Large-volume atmosphere-controlled diffraction furnace. *Meas Sci Tech* 2003;**14**:1091–8.
19. http://www.fiz-karlsruhe.de/icsd.html.
20. Morosin B, Lynch RW. Structure studies on Al_2TiO_5 at room temperature and at 600 °C. *Acta Cryst B* 1972;**28**:1040–6.
21. Bruno G, Efremov AM, Brown DW. Evidence for and calculation of micro-strains in porous synthetic cordierite. *Scripta Mater* 2010, doi:10.1016/j.scriptamat.2010.04.008.
22. Zlokazov VB, Chernyshev VV. MRIA- a program for a full profile analysis of powder multiphase neutron-diffraction time-of-flight (direct and Fourier) spectra. *J Appl Cryst* 1992;**25**:447–51.
23. Kern AA, Coelho AA. TOPAS version 2.1: General profile and structure analysis software for powder diffraction data, Bruker AXS Karlsruhe, D, 1998.
24. Aldebert P, Traverse JP. Al_2O_3: a high-temperature thermal expansion standard. *High Temp High Pressures* 1984;**16**:127–35.
25. Touloukian YS, Powell RW, Ho CY, Klemens PG. *Thermophysical properties of matter, vols. 1,2,10*. New York: Plenum Publishing; 1973.
26. Turner PS. Thermal expansion stresses in reinforced plastics. *J Res Nat Bureau of Standards* 1946;**37**:239–50.
27. Bueno S, Hernandez MG, Sanchez T, Anaya JJ, Baudin C. Nondestructive characterization of alumina/aluminium titanate composites using a micromechanical model and ultrasonic determinations. Part I: Evaluation of the effective elastic constant of aluminium titanate. *Ceram Int* 2008;**34**:181–8.
28. Pabst W, Gregorová E. New relation for the porosity dependence of the effective tensile modulus for brittle materials. *J Mater Sci* 2004;**39**:3501–3.